Int. J. Advanced Design and Manufacturing Technology, 2024, Vol. 17, No. 4, pp. 19-27

DOI: 10.71644/admt.2024.1129386 *ISSN: 2252-0406* *https://admt.isfahan.iau.ir*

Non-Linear Vibrations of Graphene Nanoplatelet-Reinforced Composite Beams using Non-Local Strain Gradient Theory

Ahmad Haghani*
Department of Mechanical Engineering,
Shahrekord branch, Islamic Azad University, Shahrekord, Iran
E-mail: a.haghani@iaushk.ac.ir, ahmad_h117@yahoo.co.uk
*Corresponding author

Received: 17 August 2024, Revised: 15 October 2024, Accepted: 2 November 2024

Abstract: With the growing integration of nanotechnology into everyday life and the importance of nanoelectromechanical systems, this article examines the non-linear free vibrations of an Euler-Bernoulli (EB) composite beam reinforced with graphene nanoplatelets (GN), considering the Non-Local Strain Gradient Theory (NLSGT). First, the elastic properties of the nanocomposite reinforced with GN were calculated using the rules of mixtures and the Halpin-Tsai (HT) model. Then, the Equations describing the motion for the EB beam were obtained through the virtual work law, the NLSGT, and the von Kármán (VK) strain field, and were analyzed through the homotopy technique. After solving the Equations, the obtained results were compared with those available in other sources, showing a very good agreement. Finally, the outcomes of varying the graphene plates (GPLs) weight fraction, the GPLs distribution, and the proportional ratio of length to thickness of the beam regarding the non-linear natural frequency (NF) were investigated where one of the important results of this paper is that the highest non-linear NF occurs first in the *X-GPLRC* distribution, then in the *A-GPLRC* distribution, and finally in the *O-GPLRC* distribution.

Keywords: Galerkin Method, GPLRC, Homotopy Analysis Method, Nonlocal Strain Gradient Theory (NLSGT)

Biographical notes: Ahmad Haghani received his PhD in Mechanical Engineering from the Science and Research Branch, Islamic Azad University, Tehran, Iran in 2017. He is currently an Assistant Professor at the Department of Mechanical Engineering, Shahrekord Branch, Islamic Azad University, Shahrekord, Iran. His current research interest includes FG-GPLRC and nonlocal strain gradient theory.

Research paper

1 INTRODUCTION

Nanoelectromechanical systems (NEMS) are considered one of the important branches of mechanical science, and beams are one of the critical components in NEMS, with widespread applications in nanocomposites. On the other hand, the classical theories in continuum mechanics have a limitation in studying the mechanical behaviour of nanostructures. These theories overlook the voids between atoms and the atomic forces within particles, which cannot be ignored in nanoscale problems. Therefore, considering the high cost of experimental studies at the nanoscale, generalized continuum mechanics theories have been proposed [1]. One such theory based on generalized continuum mechanics is the NLSGT [1-2]. Several studies have utilized this theory to solve various problems, including the following examples.

Yin and colleagues [3] investigated the vibrational behaviour of a curved nanotube subjected to supersonic airflow and internal fluid flow. They used the NLSGT to model the size-affected nanotube and derived the motion Equations through the use of Hamilton's principle (HP). To solve the Equations, the generalized differential quadrature technique was utilized.

Guo and colleagues [4] introduced a computational method to assess the non-linear electro-elastic wave scattering features in a nanoscale sandwich tube. They extracted the fundamental Equations of the problem by employing the NLSGT, HP, and the first-order shear deformation theory (FSDT). The Equations were then resolved through the finite element technique and neural networks to calculate the exact non-local functions and length scales under various conditions affecting the tube.

Biswas [5] investigated the distribution of harmonic plane waves in a non-local visco-thermo-elastic porous medium according to the NLSGT. The governing Equations were derived via the Green-Naghdi Type III model assumptions and the NLSGT. Finally, the impacts of the nonlocality length factor, viscosity, and porosity on phase speeds, damping factors, and wave infiltration depth at different frequencies were studied.

Trabelssi and colleagues [6] studied wave distribution in an EB nanobeam using the NLSGT. They employed HP to derive the beam's motion Equations and investigated the effects of the non-local factor and strain gradient (SG) factor on wave distribution. Phung-Van and colleagues [7] investigated the mechanical behavior of an FG nanosheet by employing the NLSGT. The study indicated that the mechanisms influencing stiffness in the nanoplate can be controlled by optimizing the non-local and SG factors. Liu and colleagues [8] investigated the free vibrations of an aluminum plate considering the NLSGT and molecular dynamics (MD) modelings. They calibrated the size factors in the NLSGT using MD modelings.

Singh and colleagues [9] predicted the bending specifications of an EB beam using the Moore-Gibson-Thompson thermoelasticity model along with the NLSGT. After deriving the governing Equations, they employed the Laplace transform and the wavelet estimation techniques to resolve these Equations. Behar and colleagues [10] investigated and analyzed the stability and vibrations of a rotating smart nanotube under electrical loads. They derived the boundary conditions and governing Equations using the NLSGT, EB beam theory, and HP and solved them using the Galerkin technique. Finally, they examined the impacts of the length scale of the material, non-local factors, rotational speed, boundary conditions, and external voltage on the NF.

Merzouki and Houari [11] performed an in-depth investigation of thermal vibrations in FG nanobeams, taking into account the temperature-dependent characteristics of the material. They used an extended finite element method based on the NLSGT to solve the problem and investigated 3 thermal loading categories.

Guerroudj and colleagues [12] studied the free vibrations of an FG nanobeam. They extracted the motion Equations using the higher-order SDT and the NLSGT. They also evaluated simple boundary conditions for the beam and examined the effects of structural geometry, gradient parameter, and non-local factors on the frequency of oscillation. Using nanocomposites reinforced with GN can impart diverse properties to the mechanical behavior of nanoplates and nanobeams [13]. Some of the research that has utilized these materials in the mechanical structures of nanoplates and nanobeams includes the following:

Bahranifard and colleagues [14] studied the non-linear vibration features and reactions of sandwich beams with graphene-reinforced coating layers and a porous core under moving loads. They extracted the motion Equations based on the FSDT and resolved the issues by the Newmark and Newton-Raphson methods. They found that the softening effects due to porosity rely on the arrangement of their distribution.

Safaei and colleagues [15] examined the out-of-plane free vibrations and responses to moving loads of curved sandwich beams with graphene-reinforced coating layers and a porous core. They extracted the governing Equations based on the FSDT and HP, and resolved them by differential quadrature technique and Newmark's technique. Numerical results showed that adding a small quantity of GPLs to the coating layers and core significantly changes the fundamental NF and movement ranges subject to the moving loads.

Mirzaei [16] studied the vibrations of composite plates reinforced with GN. The elasticity modulus of the plate was achieved by the HT law. The Equations governing the system were derived from the FSDT and addressed through the Ritz technique.

Ghatreh Samani and colleagues [17] investigated the free vibrations of a sandwich plate with two coating layers reinforced with GPLs. The motion Equations were established through HP and solved using the Navier technique. They ultimately examined the effect of the graphene plate pattern and their weight ratio on the natural frequencies.
Considering the research conducted on beams reinforced with GN and the NLSGT, it is evident that very few studies have been done on the use of GN combined with the NLSGT. The present work investigates the non-linear vibrations of an EB beam reinforced with carbon nanoplatelets according to the NLSGT. Initially, using the virtual work theory, classical deformation theory, NLSGT, and the VK strain field, the non-linear Equations of motion for the nanotube are derived. These Equations are then solved using the Galerkin and homotopy techniques [1]. Finally, after validating the solution, results on the variations in NF with different GPL distribution patterns, proportional ratio of length to thickness, and SG and non-local factors will be presented.

2 NON-LOCAL STRAIN GRADIENT THEORY (NLSGT)

In NLSGT [18], both the non-local elastic stress and the SG stress are considered. Therefore, the overall stress is written as follows:

$$(1-(ea)^2\nabla^2)\sigma_{xx} = E(1-l_s^2\nabla^2)\varepsilon_{xx}, \quad \nabla = \frac{\partial}{\partial x} \quad (1)$$

In this relation, E is the elastic modulus, ea is the non-local factor, and l_s is the SG length.

3 SIZE-AFFECTED EQUATIONS OF MOTION FOR AN EB BEAM

Figure 1 shows an EB beam with thickness h, length L, and width b.

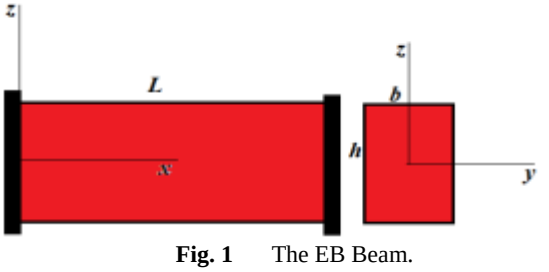

Fig. 1 The EB Beam.

The displacement field governing the EB beam is formulated as follows, where u_x is the movement along the direction of x, u_y is the movement along the direction of y, and u_z is the movement along the direction of z.

$$\begin{aligned} &u_x(x,z,t) = u(x,t) + z\frac{\partial w(x,t)}{\partial x}, \\ &u_y(x,z,t) = 0, \quad u_z(x,z,t) = w(x,t) \end{aligned} \quad (2)$$

Based on the VK strain theory and the movement field provided in "Eq. (2)", the non-linear strain field is calculated as follows.

$$\begin{aligned} &\varepsilon_{xx} = \frac{\partial u}{\partial x} + \frac{1}{2}\left(\frac{\partial w}{\partial x}\right)^2 - z\frac{\partial^2 w}{\partial x^2} \\ &\varepsilon_{xx}^{(1)} = \frac{\partial^2 u}{\partial x^2} + \frac{\partial w}{\partial x}\frac{\partial^2 w}{\partial x^2} - z\frac{\partial^3 w}{\partial x^3} \end{aligned} \quad (3)$$

To compute the motion Equations, the first-order variation of the strain energy δU, the first-order variation of the kinetic energy δK, and the first-order variation of the work done by external forces δW are first calculated. Then, using the calculus of variations and HP, the Equations of motion are derived.
The first-order variation of the strain energy δU is calculated according to the NLSGT using the subsequent Equation.
By substituting "Eq. (3) into Eq. (4)" and through the method of integration by parts, the subsequent Equation is obtained.

$$\delta U = \int_V \left(\sigma_{xx} - \nabla\sigma_{xx}^{(1)}\right)\delta\varepsilon_{xx}dV + \int_A \sigma_{xx}^{(1)}\delta\varepsilon_{xx}dA \quad (4)$$

By substituting "Eq. (3) into Eq. (4)" and using the method of integration by parts, the following Equation is obtained.

$$\begin{aligned} \delta U = {} & N\delta u|_0^L + \left(N\frac{\partial w}{\partial x} + \frac{\partial M}{\partial x}\right)\delta w\Big|_0^L - \\ & M\delta\left(\frac{\partial w}{\partial x}\right)\Big|_0^L \\ & - \int_0^L \left[\frac{\partial N}{\partial x}\delta u + \left(\frac{\partial}{\partial x}\left(N\frac{\partial w}{\partial x}\right) + \frac{\partial^2 M}{\partial x^2}\right)\delta w\right]dx \\ & - M^{(1)}\delta\left(\frac{\partial^2 w}{\partial x^2}\right)\Big|_0^L + N^{(1)}\delta\left(\frac{\partial u}{\partial x} + \frac{1}{2}\left(\frac{\partial w}{\partial x}\right)^2\right)\Big|_0^L \end{aligned} \quad (5)$$

Where N is the resultant force and M is the resultant bending moment, and they are calculated according to the subsequent Equation.

$$\begin{aligned} &N^{(0)} = \int_A \sigma_{xx}dA, \quad N^{(1)} = \frac{\partial}{\partial x}\int_A \sigma_{xx}^{(1)}dA \\ &N = N^{(0)} - \frac{\partial N^{(1)}}{\partial x} \end{aligned} \quad (6)$$

$$M^{(0)} = \int_A \sigma_{xx} z dA\,, \quad M^{(1)} = \frac{\partial}{\partial x}\int_A \sigma_{xx}^{(1)} z dA$$
$$M = M^{(0)} - \frac{\partial M^{(1)}}{\partial x} \tag{7}$$

The first-order variation of the kinetic energy δK is given by the subsequent Equation.

$$\delta K = \rho A \frac{\partial u}{\partial t}\delta u\Big|_0^L + \rho I \frac{\partial^2 w}{\partial x \partial t}\delta\left(\frac{\partial w}{\partial t}\right)\Big|_0^L + \left(\rho A \frac{\partial w}{\partial t} - \rho I \frac{\partial^3 w}{\partial x^2 \partial t}\right)\delta w\Big|_0^L - \int_0^L \left[\rho A \frac{\partial^2 u}{\partial t^2}\delta u - \left(\rho I \frac{\partial^4 w}{\partial x^2 \partial t^2} + \rho A \frac{\partial^2 w}{\partial t^2}\right)\delta w\right] dx \tag{8}$$

Where A is the area of cross-sectional and I is the moment of cross-section inertia. Additionally, the first-order variation of the work done by external forces is given by the subsequent Equation.

$$\delta W = \int_0^L q\delta w\, dx \tag{9}$$

To compute the motion Equations, HP is used, which is given by the subsequent Equation.

$$\int_{t_1}^{t_2} (\delta K - \delta U + \delta W)\, dt = 0 \tag{10}$$

Based on the above Equation and "Eqs. (6) and (7)", the boundary conditions and motion Equations, assuming zero external forces, are obtained in the following form.

$$\frac{\partial N}{\partial x} = \rho A \frac{\partial^2 u}{\partial t^2}$$
$$\frac{\partial}{\partial x}\left(N\frac{\partial w}{\partial x}\right) + \frac{\partial^2 M}{\partial x^2} = \rho A \frac{\partial^2 w}{\partial t^2} - \rho I \frac{\partial^4 w}{\partial x^2 \partial t^2}$$
$$(1-(ea)^2\nabla^2)N = A_{11} b(1-l_s^2\nabla^2)\left(\frac{\partial u}{\partial x} + \frac{1}{2}\left(\frac{\partial w}{\partial x}\right)^2\right)$$
$$(1-(ea)^2\nabla^2)M = -D_{11} b(1-l_s^2\nabla^2)\frac{\partial^2 w}{\partial x^2}$$
$$N\delta u|_0^L = 0, \quad M\delta\left(\frac{\partial w}{\partial x}\right)\Big|_0^L = 0, \quad \left(N\frac{\partial w}{\partial x} + \frac{\partial M}{\partial x}\right)\delta w\Big|_0^L = 0$$
$$N^{(1)}\delta\left(\frac{\partial u}{\partial x} + \frac{1}{2}\left(\frac{\partial w}{\partial x}\right)^2\right)\Big|_0^L = 0, \quad M^{(1)}\delta\left(\frac{\partial^2 w}{\partial x^2}\right)\Big|_0^L = 0 \tag{11}$$

In the above Equation, the stiffness coefficients A_{11} and D_{11} are calculated according to the subsequent Equation.

$$A_{11} = \sum_{i=1}^{n}\int_{h_{i-1}}^{h_i}\left(\frac{E^{(i)}}{1-(\nu^{(i)})^2}\right)dz\,, \quad D_{11} = \sum_{i=1}^{n}\int_{h_{i-1}}^{h_i}\left(\frac{E^{(i)}}{1-(\nu^{(i)})^2}\right)z^2\, dz \tag{12}$$

To obtain the differential conditions for dynamic equilibrium in terms of displacement, it is assumed that the in-plane inertia is negligible. Therefore, the first term in "Eq. (11)" can be ignored [19]. Given that the beam is clamped at both ends, the classical and higher-order boundary conditions are provided by the subsequent Equation.

$$\delta u|_0^L = 0, \quad \delta\left(\frac{\partial w}{\partial x}\right)\Big|_0^L = 0, \quad \delta w|_0^L = 0$$
$$N^{(1)}\Big|_0^L = 0, \quad M^{(1)}\Big|_0^L = 0 \tag{13}$$

Therefore, according to "Eqs. (11) and (13)", the resultant force N is calculated using the subsequent Equation.

$$N = \frac{bA_{11}}{2L}\int_0^L \left(\frac{\partial w}{\partial x}\right)^2 dx \tag{14}$$

Based on the above information, the second Equation of "Eq. (11)" is rewritten regarding the displacements as follows:

$$bD_{11}(1-l_s^2\nabla^2)\frac{\partial^4 w}{\partial x^4} - (1-(ea)^2\nabla^2)N\frac{\partial^2 w}{\partial x^2} = (1-(ea)^2\nabla^2)\left(\rho I\frac{\partial^4 w}{\partial x^2 \partial t^2} - \rho A\frac{\partial^2 w}{\partial t^2}\right) \tag{15}$$

To solve the above Equation, the function $w(x)$ is initially assumed as follows:

$$w(x,t) = \chi_m(x)\varphi_m(t) \tag{16}$$

Considering the beam's clamped ends, the function $\chi_m(x)$ is assumed as follows [19]:

$$\chi_m(x) = 1 - cos\left(\frac{2m\pi}{L}x\right) \tag{17}$$

"Eq. (16)" is substituted into "Eq. (15)", and after differentiating and using the Galerkin technique, the subsequent Equation is obtained.

$$\frac{d^2\varphi_m(t)}{dt^2} + \omega^2\left(\varphi_m(t) + \eta\left(\varphi_m(t)\right)^3\right) = 0 \tag{18}$$

$$a_1 = \int_0^L (1-(ea)^2\nabla^2)\left(\rho A\chi_m(x) - \rho I\frac{d^2\chi_m(x)}{dx^2}\right)\chi_m(x)dx \tag{19}$$

$$a_2 = \int_0^L bD_{11}(1-l_s^2\nabla^2)\frac{d^4\chi_m(x)}{dx^4}\chi_m(x)dx \tag{20}$$

$$a_3 = -\left(\frac{bA_{11}}{2L}\int_0^L \left(\frac{d\chi_m(x)}{dx}\right)^2 dx\right)\int_0^L (1 - (ea)^2\nabla^2)\frac{d^2\chi_m(x)}{dx^2}\chi_m(x)dx \quad (21)$$

$$\omega^2 = \frac{a_2}{a_1}, \quad \eta = \frac{a_3}{a_2} \quad (22)$$

"Eq. (18)" is the Duffing Differential Equation, and its general initial conditions are as follows. To find the solution to this Equation, the homotopy technique is applied.

$$\varphi_m(0) = W, \quad \left.\frac{d\varphi_m(t)}{dt}\right|_{t=0} = 0 \quad (23)$$

4 HOMOTOPY SOLUTION TECHNIQUE

The homotopy technique is considered one of the most efficient semi-analytical techniques for solving non-linear differential Equations, which has rapid and successful convergence. Generally, a non-linear differential Equation can be considered as shown below, where *N* is the non-linear operator, *g*(*x*) is the unknown operation, and *x* is the independent variable [20].

$$N[g(x)] = 0 \quad (24)$$

The homotopy combination is generally expressed by the subsequent Equation [20].

$$H[\mu(x;q); g_0(x), H(x), h, q] = (1-q)\{L[\mu(x;q) - g_0(x)]\} - qhH(x)N[\mu(x;q)] \quad (25)$$

Where $g_0(x)$ is the primary guess function for *g*(*x*), *H*(*x*) is a non-zero supplementary function, *h* is a non-zero supplementary factor, and *L* is a linear differential operator. Additionally, by varying the factor *q* from zero to one, the solution transitions from the primary guess function to the exact solution. When the right side of "Eq. (25)" is set to zero, the zero-order deformation Equation is obtained [20].

$$(1-q)\{L[\mu(x;q) - g_0(x)]\} = qhH(x)N[\mu(x;q)] \quad (26)$$

In the above Equation, if the value of *q* is set to zero, $\mu(x;0)=g_0(x)$ is obtained. Since the auxiliary function and auxiliary factor are non-zero, when *q* equals one, $\mu(x;1)=g(x)$ is obtained. Additionally, the *m*-th derivative of *g*(*x*) is calculated as follows [20]:

$$g_m(x) = \frac{1}{m!}\left.\frac{\partial^m \mu(x;q)}{\partial q^m}\right|_{q=0} \quad (27)$$

According to Taylor's theorem, the function *g*(*x*) can be expanded as a series according to the subsequent Equation.

$$g(x) \approx \sum_{k=0}^{m} g_k(x) \quad (28)$$

Additionally, the governing Equation for $g_m(x)$ is expressed as follows:

$$L[g_m(x)] = \chi_m L[g_{m-1}(x)] + hH(x)R_m(\vec{g}_{m-1}(x), x) \quad (29)$$

In the above Equation, χ_m and R_m are calculated according to the subsequent Equations.

$$\chi_m = \begin{cases} 0 & m \le 1 \\ 1 & otherwise \end{cases} \quad (30)$$

$$R_m(g_{m-1}(x), x) = \frac{1}{(m-1)!}\left\{\frac{\partial^{m-1}}{\partial q^{m-1}} N\left[\sum_{n=0}^{+\infty} g_n(x)\, q^n\right]\right\}\Big|_{q=0} \quad (31)$$

Using this method, "Eq. (18)" with the initial conditions given by "Eq. (23)" is solved [19], and the non-linear NF is calculated as follows:

$$\widetilde{\omega}^2 = \omega^2 \frac{(141\eta^2 W^4 + 384\eta W^2 + 256)}{32^2(4+3\eta W^2)^3} \quad (32)$$

"Eq. (32)" is non-dimensionalized as follows:

$$\omega^* = \sqrt{\frac{\widetilde{\omega}^2 L^4 \rho A}{b D_{11}^{(m)}}}, \quad D_{11}^{(m)} = \frac{E_m h^3}{12} \quad (33)$$

5 MECHANICAL PROPERTIES OF GPLRCS

The beam's material properties are shown in "Table 1".

Table 1 The material properties [13]

Material properties	Epoxy	GPL
E (GPa)	3.0	1010
ρ (Kg/m^3)	1200	1062.5
ν	0.34	0.186

In the present work, 3 pattern categories for the graphene-reinforced composite beam are considered. The *X* and *O* patterns represent symmetric distributions of GPLs, while the *A* pattern represents an asymmetric distribution of GPLs in the composite beam. The arrangement of these patterns is outlined in "Fig. 2".

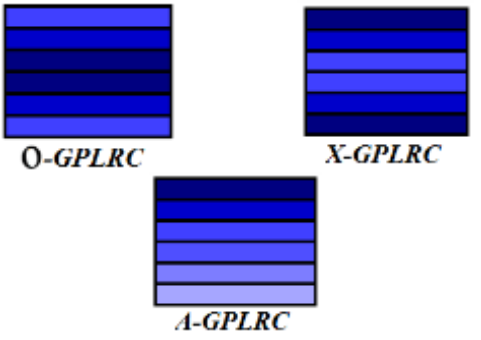

Fig. 2 Beam's GPL Distribution Patterns.

In this paper, it is assumed that N_L is an even number of layers of the graphene-reinforced composite. V_{GPL} is the GPLs volume fraction, which is computed for various patterns through the subsequent Equations [13].

$$X-GPLRC: V_{GPL}^{(i)} = 2\hat{V}_{GPL}\frac{|2i-N_L-1|}{N_L} \quad (34)$$

$$O-GPLRC: V_{GPL}^{(i)} = 2\hat{V}_{GPL}\left(1-\frac{|2i-N_L-1|}{N_L}\right) \quad (35)$$

$$A-GPLRC: V_{GPL}^{(i)} = \hat{V}_{GPL}\frac{|2i-1|}{N_L} \quad (36)$$

In these Equations, $V_{GPL}^{(i)}$ is the GPLs volume fraction for the *i*-th beam layer. $\hat{V}_{GPL}$ is the total GPLs volume fraction in the beam, and it is computed through the subsequent Equation, where W_{GPL} is the total GPLs weight fraction in the beam [13].

$$\hat{V}_{GPL} = \frac{W_{GPL}}{W_{GPL}+(1-W_{GPL})\left(\frac{\rho_{GPL}}{\rho_m}\right)} \quad (37)$$

To compute the effectiveness of each layer Young's modulus of the graphene-reinforced composite beam, the altered HT micromechanics framework is employed, which is expressed by the subsequent Equation [17].

$$E^{(i)} = \frac{3}{8}\left(\frac{1+\xi_L\eta_L V_{GPL}^{(i)}}{1-\eta_L V_{GPL}^{(i)}}\right)E_m + \frac{5}{8}\left(\frac{1+\xi_T\eta_T V_{GPL}^{(i)}}{1-\eta_T V_{GPL}^{(i)}}\right)E_m \quad (38)$$

$$\eta_L = \frac{\left(\frac{E_{GPL}}{E_m}\right)-1}{\left(\frac{E_{GPL}}{E_m}\right)+\xi_L}, \quad \eta_T = \frac{\left(\frac{E_{GPL}}{E_m}\right)-1}{\left(\frac{E_{GPL}}{E_m}\right)+\xi_T}$$

In the above Equation, ξ_L and ξ_T are the GPLs geometric factors, which are computed using the subsequent Equation. In this Equation, t_{GPL} b_{GPL}, and a_{GPL} are the thickness, width, and length of the GPL nanofillers, sequentially.

$$\xi_L = 2\left(\frac{a_{GPL}}{t_{GPL}}\right), \quad \xi_T = 2\left(\frac{b_{GPL}}{t_{GPL}}\right) \quad (39)$$

Based on the mixtures rule, for each layer of the graphene-reinforced composite beam, the density $\rho^{(i)}$ and Poisson's ratio $v^{(i)}$ are computed using the subsequent Equations. In these Equations, $V_m^{(i)} = 1 - V_{GPL}^{(i)}$ is the matrix volume fraction for every layer.

$$\rho^{(i)} = \rho_m V_m^{(i)} + \rho_{GPL} V_{GPL}^{(i)} \quad (40)$$

$$v^{(i)} = v_m V_m^{(i)} + v_{GPL} V_{GPL}^{(i)} \quad (41)$$

6 ASSESSMENT OF SOLUTION INDEPENDENCE WITH RESPECT TO THE NUMBER OF LAYERS

Figure 3 illustrates the alteration of the dimensionless non-linear NF ω^* with respect to the maximum non-dimensional transverse displacement $W^*=W/h$ for the case, where $\lambda_{NL}=ea/L=0.01<\lambda_{SG}=l_s/L=0.02$ and with an *X-GPLRC* distribution. Table (1) provides the mechanical specifications, with $L/h=20$ and the number of layers ranging from 6 to 14.

As can be seen from the graph, the curves for 10 to 14 layers converge, indicating that the solution becomes independent of the number of layers for 10 or more layers.

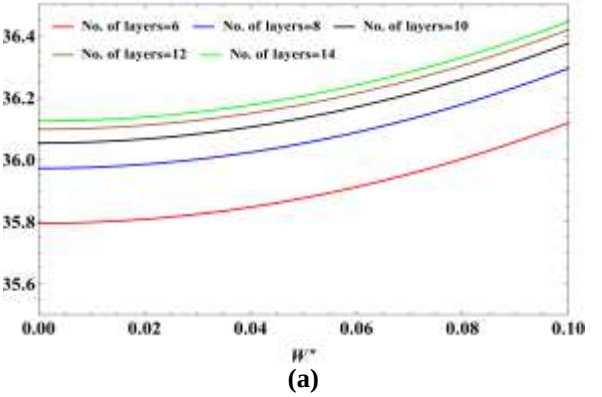

(a)

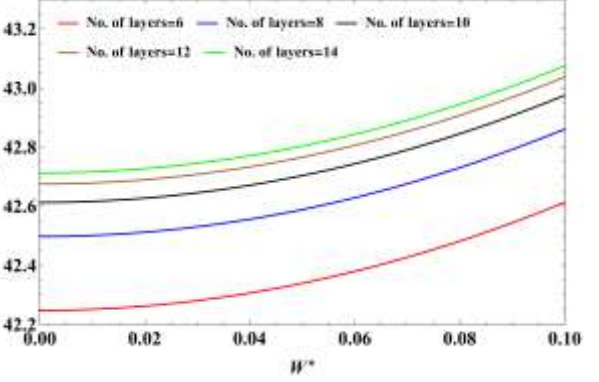

(b)

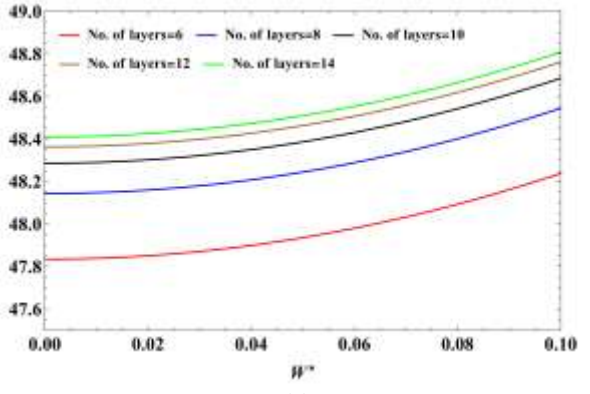

(c)

Fig. 3. Variation of the dimensionless non-linear NF regarding the maximum non-dimensional transverse displacement of the beam for (a) W_{GPL}=0.3%, (b) W_{GPL}=0.5%, and (c) W_{GPL}=0.7% for various numbers of layers.

7 SOLUTION VALIDATION

To validate the solution for an isotropic material, the results of the dimensionless non-linear NF ω^* regarding the maximum non-dimensional transverse displacement W^* are compared with the results of Faghidian [19] for two cases: λ_{NL}=0.01<λ_{SG}=0.02 and λ_{NL}=0.02>λ_{SG}=0.01, assuming L/h=20. The comparison shows very good agreement. Figure (4) illustrates the result of this comparison.

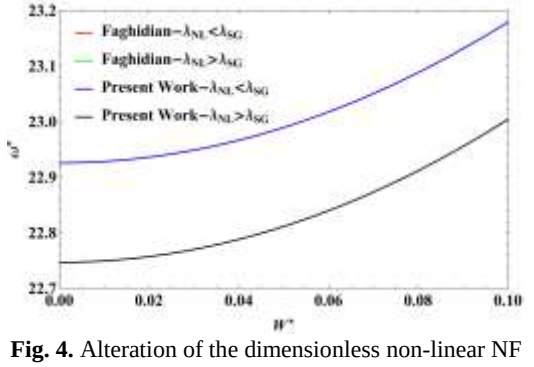

Fig. 4. Alteration of the dimensionless non-linear NF regarding the maximum non-dimensional transverse movement of the beam.

8 RESULTS AND DISCUSSION

In this section, the effects of variations in W_{GPL}, non-local factors, the SGT, and the ratio L/h on the dimensionless non-linear NF are examined. Table 1 provides the mechanical specifications considered for the present work. Figure 5 illustrates the impact of varying W_{GPL} on the dimensionless non-linear NF for *O-*, *X-*, and *A-GPLRC* distributions with L/h=20.

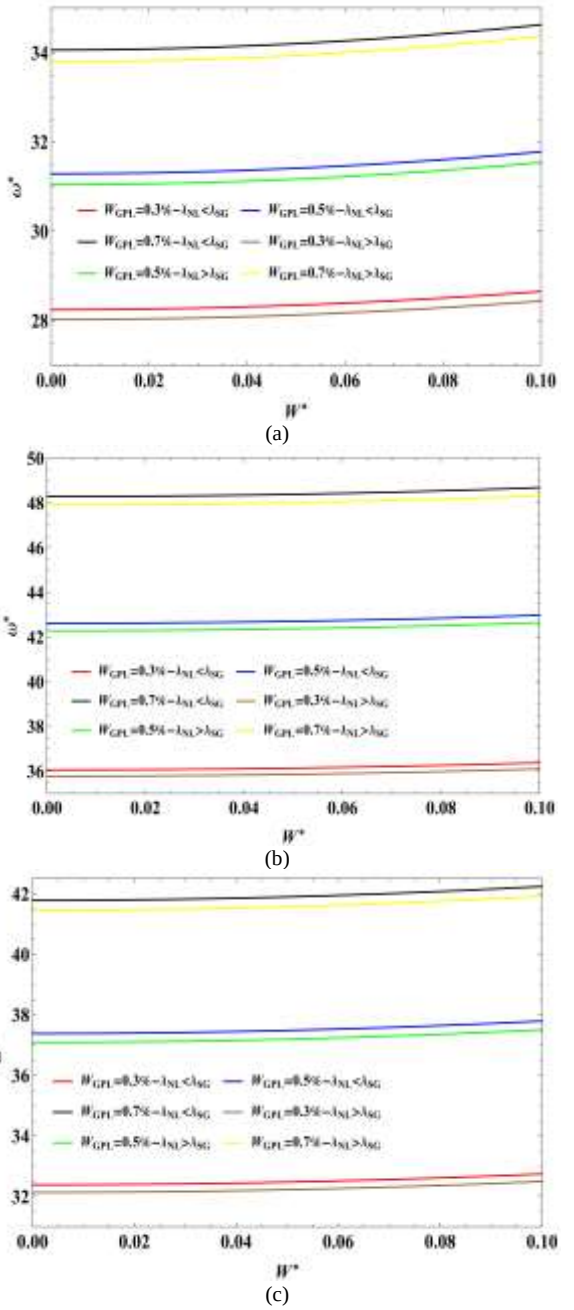

Fig. 5 Effect of varying W_{GPL} on the dimensionless non-linear NF for: (a): O-GPLRC, (b): X-GPLRC, and (c): A-GPLRC distributions.

As illustrated in the Figure, increasing W_{GPL} from 0.3% to 0.7% results in a rise in the NF. This can be attributed to the ibeam's enhanced rigidity as W_{GPL} increases for all three GPL distributions. Additionally, the NF is higher in the case where λ_{NL} =0.01<λ_{SG} =0.02 compared to when λ_{NL} =0.01>λ_{SG} =0.02. Moreover, the highest dimensionless non-linear NF occurs first in the *X-GPLRC* distribution, then in the *A-GPLRC* distribution, and finally in the *O-GPLRC* distribution. Figure 6 illustrates the effect of changing the L/h ratio on the

dimensionless non-linear NF for *O-GPLRC*, *X-GPLRC*, and *A-GPLRC* distributions, with W_{GPL} =0.5% and λ_{NL} =0.01<λ_{SG} =0.02. As seen from the figure, for all three distributions, *O-GPLRC*, *X-GPLRC*, and *A-GPLRC*, the dimensionless non-linear NF reduces with rising *L*/*h* ratio.

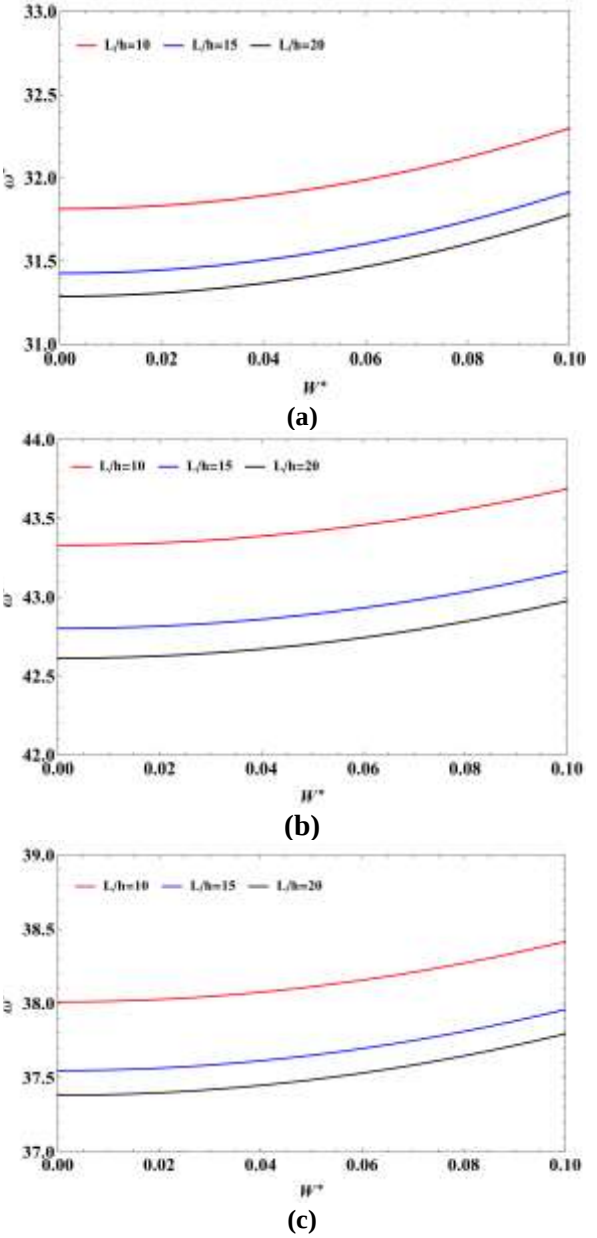

Fig. 6 Impact of varying *L/h* ratio on the dimensionless non-linear NF for: (a): O-GPLRC, (b): X-GPLRC, and (c): A-GPLRC distributions.

9 CONCLUSIONS

The present work investigates the non-linear free vibrations of EB beams reinforced with GN, considering the NLSGT. The elastic properties of the graphene nanoplatelet-reinforced nanocomposites were computed through the mixtures rule and the HT model. The governing Equations for the EB nanobeam were extracted through the virtual work law, NLSGT, and the VK strain field. Finally, the governing Equations were solved through the homotopy technique, and the impacts of varying GPL weight fraction, GPL distribution patterns, and the *L*/*h* ratio on the non-linear NF were examined. A summary of the findings is as follows:

- For all three GPL distributions, increasing W_{GPL} yields in rising in the non-linear NF. This results from the increased beam stiffness caused by the higher W_{GPL}.
- The NF is higher when $\lambda_{NL}<\lambda_{SG}$ compared to when $\lambda_{NL}>\lambda_{SG}$.
- The highest non-linear NF occurs first in the *X-GPLRC* distribution, then in the *A-GPLRC* distribution, and finally in the *O-GPLRC* distribution.
- In all three GPL distributions, the non-linear NF reduces with a rise in the *L*/*h* ratio.

10 NOMENCLATURE

Parameters	Definition
E	Elastic modulus
ρ	Density
ν	Poisson's ratio
ω^*	non-dimensional natural frequency
V	Volume fraction
W	Weight fraction
ea	non-local factor
l_s	SG length

REFERENCES

[1] Haghani, A., Jahangiri, M., and Ghaderi, R., Nonlinear Vibrations of Timoshenko Nanobeam Using Stress Driven Nonlocal Theory, Physica Scripta, Vol. 97, No. 7, 2022, pp. 095206.

[2] Zaera, R., Serrano, Ó., and Fernández-Sáez, J., On the Consistency of The Nonlocal Strain Gradient Elasticity, International Journal of Engineering Science, Vol. 138, 2019, pp. 65-81.

[3] Yin, J., Zou, Y., Li, J., Zhang, W., Li, X., and Habibi, M., Dynamic Stability and Frequency Responses of The Tilted Curved Nanopipes in A Supersonic Airflow via 2D Hybrid Nonlocal Strain Gradient Theory, Engineering Structures, Vol. 301, 2024, pp.117240.

[4] Guo, Y., Maalla, A., and Habibi, M., Electroelastic Wave Dispersion in The Rotary Piezoelectric NEMS Sensors/Actuators via Nonlocal Strain Gradient Theory,

Mechanical Systems and Signal Processing, Vol. 216, 2024, pp.111453.

[5] Biswas, S., The Propagation of Plane Waves in Nonlocal Visco-Thermoelastic Porous Medium Based on Nonlocal Strain Gradient Theory, Waves in Random and Complex Media, Vol. 34, No. 1, 2024, pp.372-403.

[6] Trabelssi, M., El-Borgi, S., and Friswell, M. I., Application of Nonlocal Strain Gradient Theory for The Analysis of Bandgap Formation in Metamaterial Nanobeams, Applied Mathematical Modelling, Vol. 127, 2024, pp. 281-296.

[7] Phung-Van, P., Hung, P. T., Nguyen-Xuan, H., and Thai, C. H., Small Scale Analysis of Porosity-Dependent Functionally Graded Triply Periodic Minimal Surface Nanoplates Using Nonlocal Strain Gradient Theory, Applied Mathematical Modelling, Vol. 127, 2024, pp. 439-453.

[8] Liu, C., Yu, J., Zhang, B., and Zhang, C., Size Parameter Calibration of Nonlocal Strain Gradient Theory Based on Molecular Dynamics Simulation of Guided Wave Propagation in Aluminum Plates, Thin-Walled Structures, Vol. 198, 2024, pp. 111659.

[9] Singh, B., Jangid, K., and Mukhopadhyay, S., Implementation of Legendre Wavelet Method for The Size Dependent Bending Analysis of Nano Beam Resonator Under Nonlocal Strain Gradient Theory, Computers & Mathematics with Applications, Vol. 153, 2024, pp. 94-107.

[10] Behar, M., Boukhalfa, A., and Aouinat, A. L., Examining the Critical Speed and Electro-Mechanical Vibration Response of a Spinning Smart Single-Walled Nanotube Via Nonlocal Strain Gradient Theory, Mechanics of Advanced Materials and Structures, 2024, pp. 1-17.

[11] Merzouki, T., Houari, M. S. A., Nonlocal Strain Gradient Theory for Free Vibration Analysis of FG Nano-scale Beams in Thermal Environments Using an Efficient Numerical Model, Journal of Vibration Engineering & Technologies, 2024, pp. 1-26.

[12] Guerroudj, M., Drai, A., Daikh, A. A., Houari, M. S. A., Aour, B., Eltaher, M. A., and Belarbi, M. O., Size-Dependent Free Vibration Analysis of Multidirectional Functionally Graded Nanobeams Via a Nonlocal Strain Gradient Theory, Journal of Engineering Mathematics, Vol. 146, No. 1, 2024, pp. 20.

[13] Haghani, A., Kiani, Y., Closed Form Expressions for Nonlinear Analysis of FG-GPLRC Beam Under Thermal Loading: Thermal Postbuckling and Nonlinear Bending, International Journal of Structural Stability and Dynamics, Vol. 24, No. 2, 2024, pp. 2450016.

[14] Bahranifard, F., Malekzadeh, P., and Golbahar Haghighi, M. R., Large Amplitude Vibration of Sandwich Beams with GPLRC Face Sheets and Porous Core Under Moving Load, Mechanics Based Design of Structures and Machines, Vol. 52, No. 3, 2024, pp. 1627-1650.

[15] Safaei, M., Malekzadeh, P., and Haghighi, M. G., Out-of-Plane Moving Load Response and Vibrational Behavior of Sandwich Curved Beams with GPLRC Face Sheets and Porous Core, Composite Structures, Vol. 327, 2024, pp. 117658.

[16] Mirzaei, M., Vibration Characteristics of Sandwich Plates with GPLRC Core and Piezoelectric Face Sheets with Various Electrical and Mechanical Boundary Conditions, Mechanics Based Design of Structures and Machines, Vol. 52, No. 2, 2024, pp. 990-1013.

[17] Ghatreh Samani, S., Beheshti, H., Akbarzadeh, A. H., and Kiani, Y., Frequency Assessment of Sandwich Rectangular Plates with an Anisogrid Core and GPLRC Face Sheets, International Journal of Structural Stability and Dynamics, 2024, pp. 2550175.

[18] Lim, C. W., Zhang, G., and Reddy, J., A Higher-Order Nonlocal Elasticity and Strain Gradient Theory and Its Applications in Wave Propagation, Journal of the Mechanics and Physics of Solids, Vol. 78, 2015, pp. 298-313.

[19] Faghidian, S. A., Reissner Stationary Variational Principle for Nonlocal Strain Gradient Theory of Elasticity, European Journal of Mechanics-A/Solids, Vol. 70, 2018, pp. 115-126.

[20] Liao, S., Advances in the Homotopy Analysis Method, World Scientific, China, 2013, pp. 1-35, 978-9814551243.